

# Cumulative all-optical switching in Co/Pd superlattices

F. Hoveyda, E. Hohenstein, and S. Smadici

*Department of Physics and Astronomy, University of Louisville, KY 40292, USA*

Cumulative all-optical switching was observed in Co/Pd superlattices. Lattice is part of the process for our experimental conditions. A minimal model of reversal by domain wall motion is presented, which qualitatively explains the features observed.

## I. INTRODUCTION

In ultrafast all-optical switching (AOS) of ferrimagnetic rare earth (RE)- transition metal (TM) alloys<sup>1</sup> the magnetization is reversed by 180 degrees. In contrast to experiments on iron garnet crystals<sup>2,3</sup>, no external magnetic field  $H_{ext}$  is required to prevent nucleated domains from collapsing. This reversal was examined in detail and both polarization-independent and polarization-dependent switching have been reported<sup>4,5</sup>. It is remarkable that partial ultrafast reversal in RE-TM alloys is observed within 1  $ps$ , much less than typical precession periods. As also observed with electron beam fields<sup>6</sup>, the macrospin of the Landau-Lifshitz-Gilbert (LLG) equation fragments in the intense applied laser field. However, it reassembles in the opposite direction through an intermediate ferromagnetic state. Models of magnetization time dependence apply the Landau-Lifshitz-Bloch (LLB) equations accounting for the variation in macrospin magnitude<sup>7</sup> or microscopic atomistic calculations with exchange interactions<sup>8,9</sup>.

In addition, AOS was observed in ferromagnetic Co/Pt superlattices<sup>10,11</sup>. For ferromagnetic Co/Pd superlattices, regular thermal demagnetization patterns have been obtained with 12  $ns$  pulses<sup>12</sup>.

In this work, we scanned an ultrafast high-repetition rate laser field on Co/Pd superlattices. Cumulative polarization-independent AOS was observed. Examination of polarizing and magnetic microscopy images showed the importance of thermal and long-range processes. In our experimental conditions the reversal is initiated after a few  $ms$ . The lattice is participating in the reversal process. A minimal model is presented and applied to a qualitative interpretation of the results.

## II. EXPERIMENTS

### A. Samples and experimental setups

The [Co/Pd] multilayer samples *A* and *B* were grown by e-beam evaporation at room temperature. Before the deposition, the Corning white-water glass substrates were immersed in Nanostrip solution for five minutes, placed in acetone and then methanol, and sonicated in each liquid for 10 minutes at 60 °C. The deposition was carried out at  $2 \times 10^{-6}$  Torr pressure with the substrate at an angle of 45° to the incident beam. The substrate rotated

around its normal at 5 *RPM* during deposition. The target multilayer structure was 4 x [Co/Pd] with 0.7 nm thick Co and 1 nm thick Pd layers. The total thicknesses measured with AFM were 4.1 nm and 6.2 nm for samples *A* and *B*. Sample *A* is thinner because it was placed further out from the crucibles during deposition.

MOKE measurements were performed in both longitudinal and polar geometry. The variable-temperature setup consisted of a HeNe laser, rotatable Glan-Thompson polarizer and analyzer, photoelastic modulator (PEM), an electromagnet (GMW) driven by a bipolar power supply (KEPCO BOP 50-8ML), and a photodiode detector connected to a lock-in amplifier. The sample was mounted on an Al holder and placed at the center of the electromagnet. The incident beam was *p*-polarized and was focused on the sample. The incidence angle in the L-MOKE geometry was 25 deg. The reflected beam from sample surface passed through the PEM (Hinds PEM-90) and analyzer. The hysteresis loop was obtained by averaging the results from running a sixteen-cycle waveform. L-MOKE showed an in-plane easy axis with  $H_c = 47$  *Oe* for sample *A* and  $H_c = 141$  *Oe* for sample *B* [Fig. 1(a)]. P-MOKE showed hard axis hysteresis loops.

The fluence of an ultrafast TiS laser with 120 *fs* pulses at 800 *nm* wavelength and a repetition rate of 80 *MHz* was adjusted by a combination of a polarizing cube and a half-wave plate (HWP) attached to a motorized rotation stage [Fig. 1(b)]. A quarter-wave plate (QWP) was applied to modify the beam polarization. The laser beam was focused to a typical size of 25  $\mu m$ . The sample was AC demagnetized before the writing, to increase the number of magnetic domains, and was scanned along the two directions orthogonal to the beam using two motorized stages. The writing speed  $v$  was varied between 0.1  $mm/s$  and 10  $mm/s$ . A small beam asymmetry could be removed by placing a blade before the lens to partially cut the beam.

The sample response to TiS laser scans was examined with polarizing and magnetic force microscopy (MFM). Polarizing microscopy imaging in transmission mode was carried out with a Zeiss Imager microscope. The polarizer and rotatable analyzer were crossed, then offset a small angle in both directions. The images were then subtracted to enhance the birefringent contrast. Images were also made with the polarizer and analyzer removed.

Magnetic domains were imaged using an Asylum Research MFM (MFP-3D-BIO) with a low moment tip from Nanosensors (SSS-MFMR). It was operated in tapping mode at a lift height of 50 nm. Before imaging, the tip

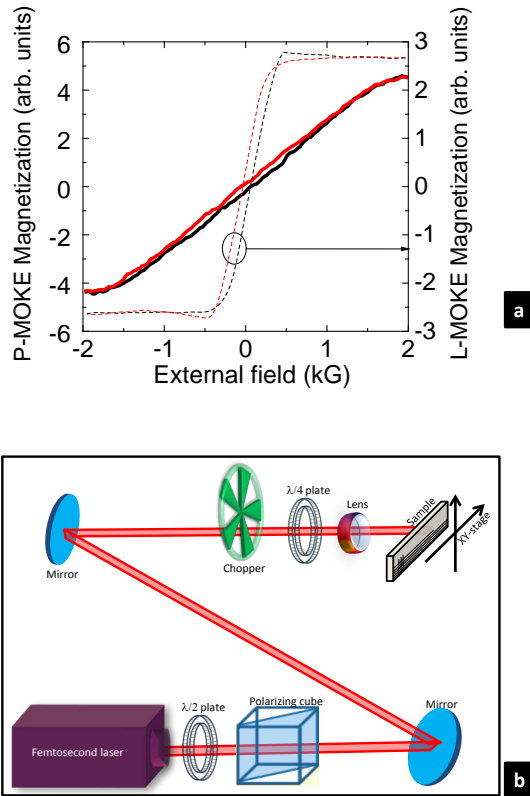


FIG. 1: (a) L- and P-MOKE hysteresis loops for sample A. (b) Sketch of the writing setup.

was magnetized with a permanent magnet attached to a moving stage.

## B. Results

Polarizing microscopy images show irregular angular domains before writing [Fig. 2(a)]. Patterns made during the writing procedure appear as “stripes” in the images. A birefringent contrast at the stripe center is visible after writing [Fig. 2(b)]. This contrast is magnetic, not structural, because it matches the background magnetic domain contrast and angular shape. The contrast is not changed with an azimuthal sample rotation, pointing to reversed magnetic domains with magnetization oriented perpendicular to the surface. Reversals with the magnetization pointing down on a magnetization-up background were also observed (not shown).

Additional small domains are observed at the center of reversed stripes written at lower speed [Fig. 2(c)]. Unlike the small linear defects induced by a laser beam in glass<sup>13,14</sup>, their orientation does not change with rotation of laser polarization. Further increases in fluence give a thermal demagnetization speckle pattern (not shown) at stripe center. The low-fluence features are no longer vis-

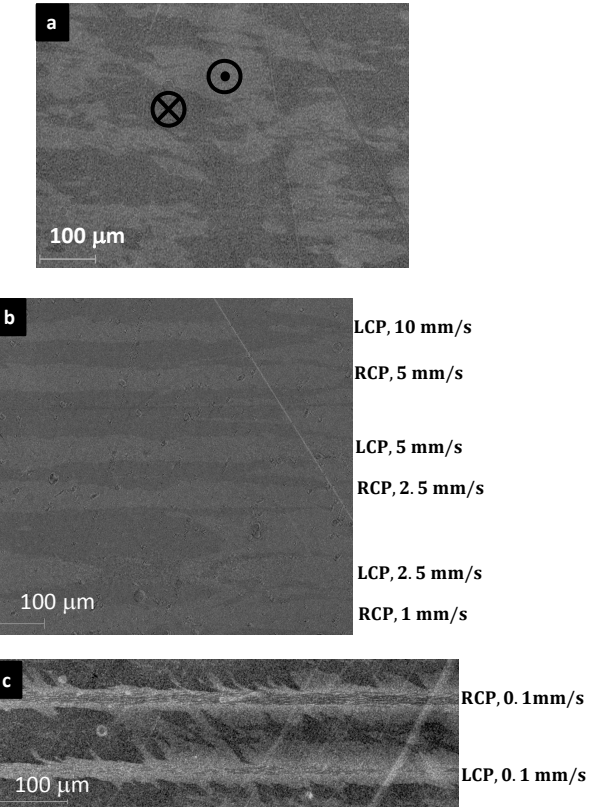


FIG. 2: (a) Background domains of sample A. (b) AOS in sample A at 150 mW power. (c) Nucleation of a second domain in sample A at 125 mW power and smaller speed.

ible in the thermally demagnetized regions, unlike what would be expected of structural changes, further supporting their magnetic origin.

Two types of AOS have so far been observed in ferromagnetic materials: single- and multiple-pulse (“cumulative”) switching. At a typical writing speed  $v = 5 \text{ mm/s}$  and beam diameter  $D = 25 \mu\text{m}$ ,  $4 \times 10^5$  consecutive pulses are incident on the sample before the beam moves away. Therefore, the observed AOS in Co/Pd is cumulative. Similar results are obtained with right- (RCP), left- (LCP) and linearly-polarized (LP) light, supporting a thermal model for cumulative switching in Co/Pd superlattices. This is in contrast to cumulative switching in Co/Pt superlattices, in which the magnetization was reversed with RCP or LCP light and absent with LP light<sup>11</sup>.

Observations also point toward the relevance of long-range magnetic interactions. Fluence decreases gradually toward the wings of the beam profile, from a maximum  $F_{max}$  at the center [Fig. 3(a), inset]. The same sequence of final states is expected across one stripe, with fluence decreasing down from a maximum  $F_{max}$ , as in images of a stripe center made at different powers. Similar results were observed. For instance, the narrowest magnetic domains near the stripes [Fig. 3(a)] are reversed regions, corresponding to regions at the center of the stripe in Fig.

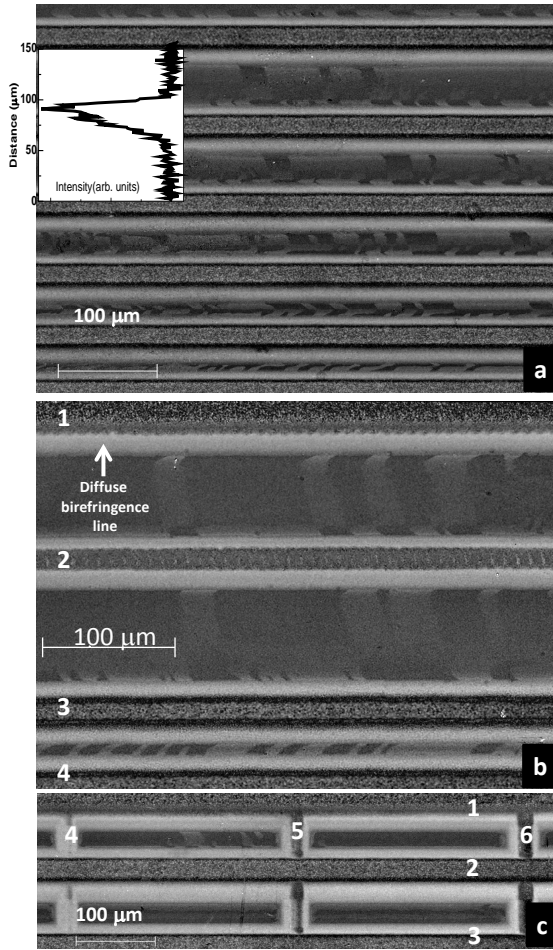


FIG. 3: Polarizing microscopy images of sample *B*. (a) AOS domains extend away from under the laser beam profile (top) and show complementary contrast at small stripe spacing (bottom). All stripes were written with 600 mW power, LP light, and at 10 mm/s speed. (b) Opposite reversal across a stripe. Writing parameters are (380 mW, LCP, 1 mm/s) for 1, (220 mW, LCP, 1 mm/s) for 2, (600 mW, LP, 10 mm/s) for 3 and 4. (c) Example of regular reversed domains. Writing parameters are (700 mW, LP, 2.5 mm/s) for 1, (700 mW, LP, 5 mm/s) for 2, (500 mW, LP, 5 mm/s) for 3, (200 mW, LCP, 2.8 mm/s) for 4, (235 mW, LCP, 2.8 mm/s) for 5, and (270 mW, LCP, 2.8 mm/s) for 6.

2. However, for widely-spaced stripes, images also show longer range domains, extending far away from areas exposed to the beam [Fig. 3(a), top part]. Complementary domain contrast is also observed for closely-spaced stripes [Fig 3(a), lower part] and for domains on opposite sides of one stripe [Fig. 3(b)]. Domains can be made regular in areas surrounded by stripes on all sides [Fig. 3(c)]. This suggests that the long-range demagnetization fields  $H_{DM}$  should be considered.

MFM measurements gave further insight into the magnetic structure. Small domains are oriented with magnetization perpendicular to the surface at stripe center (Fig. 4), consistent with previous results<sup>12</sup>. Surprisingly,

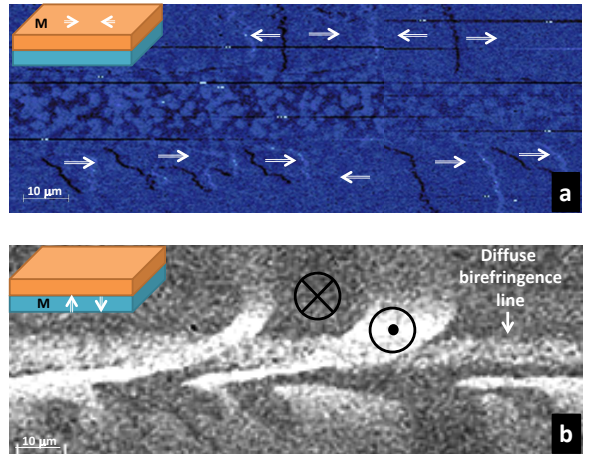


FIG. 4: MFM (a) and polarizing microscopy (b) images of a stripe in sample *B* (100 mW, LP, 10 mm/s). The arrows show the direction of magnetization. Inset: sketch of a side view of the magnetic structure.

additional in-plane domains were observed toward the edges, of the same shape as the out-of-plane domains of polarizing microscopy. This shows that the magnetic structure is not uniform within the sample (Fig. 4, insets). The top layer in-plane magnetization is probed in MFM, but not in polarizing microscopy at normal incidence (the higher-order Voigt effect is neglected), while a buried layer out-of-plane magnetization, not visible in MFM, appears in transmission polarizing microscopy.

A strong interlayer coupling is suggested by a comparison of MFM and polarizing microscopy images, with the magnetizations of the buried and surface layers locked into a fixed relative orientation. A rotation of the total sample magnetization as a unit explains the in-plane easy axis in L-MOKE and the hard-axis features in P-MOKE measurements [Fig. 1(a)].

The orientation of the domain walls (DW) in the immediate vicinity of the stripe makes an “arrow” pointing opposite the sample scanning direction and in the direction of the apparent laser spot motion on the sample (Fig. 5). This suggests that DW processes should be considered in a reversal model. The DW may change direction further away from the stripe [Fig. 3(b)], from a residual in-plane magnetic anisotropy induced during deposition.

A diffuse bright birefringent contrast near the thermal demagnetization areas, without the angular edges of magnetic domains, is also visible in polarizing microscopy images (Fig. 3). Unlike the magnetic domains, this birefringence contrast changes sign with sample rotation with a period consistent with structural birefringence of the glass substrate<sup>15,16</sup>. This feature is absent in MFM images [Fig. 4(a)], but present in the polarizing microscopy image [Fig. 4(b)], also consistent with a substrate location.

Measurements were made with a chopped beam, re-

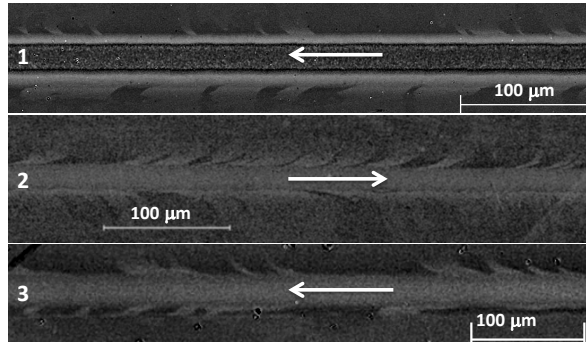


FIG. 5: Domain walls are oriented differently, depending on the scan direction, shown by the arrow. Writing parameters are (sample B, 600 mW, LCP, 10 mm/s), (sample A, 125 mW, RCP, 10 mm/s), and (sample A, 190 mW, RCP, 10 mm/s), for stripe 1, 2, and 3, respectively.

sulting in sequences of “dots”. The magnetic features in polarizing microscopy images show a filamentary structure with front-back asymmetry, offset in the scanning direction with respect to the diffuse background (Fig. 6). The spatial offset points to a delay on the order of  $\sim \frac{25 \mu m}{5 mm/s} = 5 ms$  in initiation of magnetization switching. It shows that a slow process is part of the complete reversal.

### III. DISCUSSION

#### A. Coherent rotation

A minimal model, including thermal processes and long-range magnetic interactions, describes qualitatively our observations. We consider first traditional coherent rotation models of reversal, based on the LLG equation, with a constant total magnetization magnitude  $|\vec{M}|$

$$\frac{d\vec{M}}{dt} = -\gamma \vec{M} \times \vec{H}_{eff} + \frac{\alpha}{M_s} \vec{M} \times \frac{d\vec{M}}{dt} \quad (1)$$

$\vec{M}$  is the sum of the coupled layer magnetizations. We assume that the interlayer magnetic coupling is strong, so that the total magnetization rotates as a unit, as suggested by the MOKE results and polarizing and MFM images. The effective field  $\vec{H}_{eff} = \vec{H}_A + \vec{H}_{DM} + \vec{H}_{ext}$  is the sum of an anisotropy field  $\vec{H}_A$ , a demagnetization field  $\vec{H}_{DM} = 4\pi M_s \cos(\theta)$  (emu units) for a thin film, and an external field  $\vec{H}_{ext}$ . We have  $H_{ext} = 0$  because no external bias field is applied and the light magnetic field is negligible for our fluence.

A time-dependent  $\vec{H}_{eff}$  can give very complex solutions of Eq. (1), including  $\vec{M}$  switching between local energy minima separated by 180 degrees [Fig. 7(a)]. A

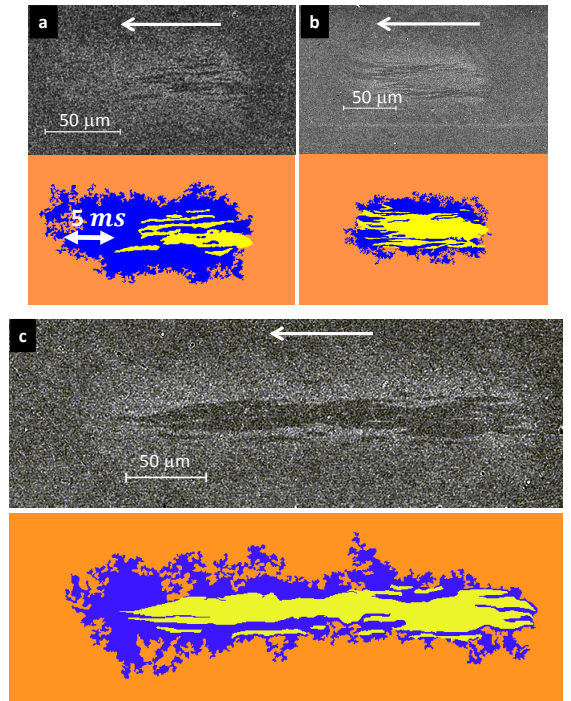


FIG. 6: Magnetic dots made with chopped beams show a delay in the onset of reversal. These stripes were written in sample A. The writing parameters were ( $f = 20 Hz$ , 230 mW, LCP, 5 mm/s), ( $f = 10 Hz$ , 230 mW, LCP, 2.5 mm/s) and ( $f = 10 Hz$ , 230 mW, RCP, 10 mm/s), for (a), (b) and (c), respectively. The arrows show the scan direction.

variable  $\vec{H}_{eff}$  can arise from a variable  $\vec{H}_A$ ,  $\vec{H}_{DM}$  or  $\vec{H}_{ext}$ . For instance, the Ni magnetization can be set to precesses around a new equilibrium direction after  $\vec{H}_A$  has been changed<sup>21</sup>. The demagnetization field  $\vec{H}_{DM}$  can also acquire a time dependence. For instance, a variable  $\vec{H}_{DM}$  has been proposed as a hard-axis out-of-plane pulsed field, rotating the in-plane magnetization of a film by precession<sup>24,25</sup>. Switching with a time-dependent  $H_{ext}$  from currents<sup>26</sup> or high-fluence lasers<sup>27</sup> has also been observed.

We can exclude the third possibility. A variable  $\vec{H}_A$  or  $\vec{H}_{DM}$  can arise from thermal effects and heat accumulation. However, the presence of DW and the relatively long timescales support a reversal by DW motion in our case, rather than by coherent rotation.

#### B. Domain walls

The LLG equation describes a reversal by coherent rotation of magnetization. This is justified at short timescales, as DW are moving too slowly. The dependence of DW orientation on scan direction (Fig. 5) and the long time-scale filamentary structure in dot images (Fig. 6) suggest that DW processes should be included

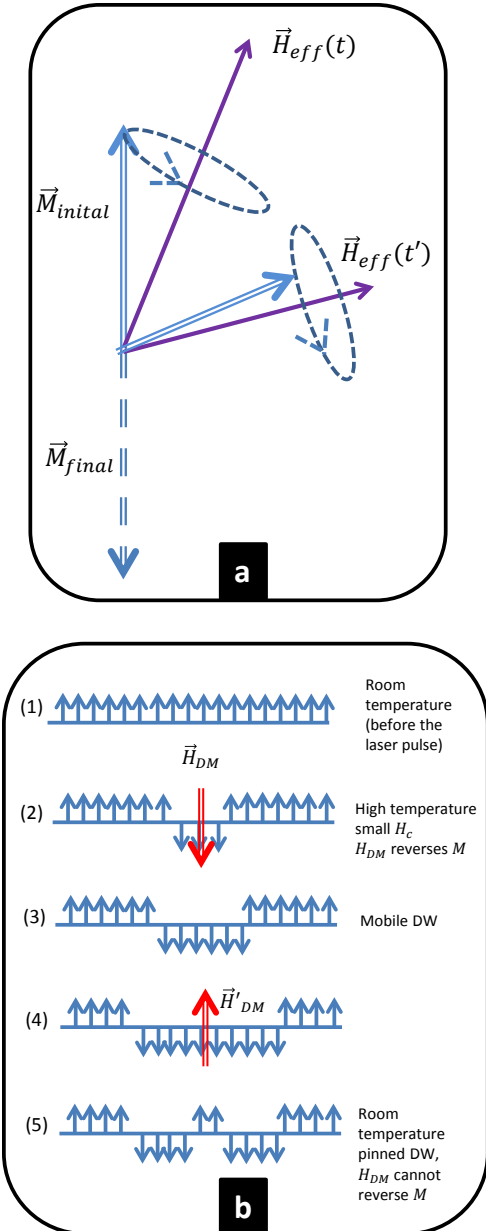


FIG. 7: (a) Reversal in LLG models with  $H_{eff} \neq \text{const}$  and  $M$  rotation by 180 degrees between two equivalent energy minima. (b) Reversal by DW motion. Sketch of domain nucleation and DW propagation for the buried layers.  $H_{DM}, H'_{DM}$  are demagnetization fields. The domain is nucleated in (2), expands (3), and a second domain may be nucleated (5), as in Fig. 2(c). The in-plane magnetization of the surface layer can be rotated by precession around  $H_{DM}$ .

in a model of AOS in Co/Pd. We consider a reversal by DW motion.

To include DW processes, we may consider first a circular magnetic domain of radius  $r_0$  and thickness  $h$ . The energy of a domain with magnetization perpendicular to the surface in the limit  $r_0 \gg h$  and in the absence of an

external field is (emu units)<sup>28</sup>

$$E_T = 2\pi r_0 h \sigma_w - 4r_0 h^2 (2\pi M_s^2) \ln\left(\frac{8r_0}{h}\right) \quad (2)$$

The first term is the domain wall energy and the second is the demagnetization field (shape anisotropy) energy. The logarithm is related to the circular geometry. The first term tends to decrease the domain size, while the second term tends to increase it.

The non-uniform fluence of the beam profile and in-plane heat diffusion give variable electron  $T_e$ , lattice  $T_p$  and spin  $T_s$  profiles in the sample plane. In three-temperature (3T) models of magnetization dynamics, heat is initially deposited in the metallic superlattice electron reservoir by absorption. It is transferred to the lattice within a few ps, increasing its temperature  $T_p$ . For magnetic materials a temperature  $T_s$  of the spin reservoir is also introduced.  $T_e$  and  $T_s$  have strong variations over a few ps, after which all three temperatures are the same, gradually decreasing toward the initial temperature. The 3T models with microscopic spin-flip scattering processes describe well the ultrafast demagnetization<sup>17-19</sup>.

The 12.5 ns time interval between pulses at our repetition rate is smaller than the cooling time and there is insufficient time for the material to cool back after each pulse. This gives heat accumulation<sup>20</sup>, which has been confirmed in our samples in separate pump-probe experiments (not shown). It can explain the delay in the onset of AOS (Fig. 5), when energy has first to be deposited in the structure for switching to occur.

The non-uniform temperature  $T$  profile, where  $T = T_p = T_s = T_e$  after a few ps in 3T models, and the magnetic domain energy suggest a mechanism for nucleation of domains [Fig. 2(a)] and propagation of domain walls [Fig. 3(a)].

To nucleate a domain, we can consider a modified version of the model for ferrimagnetic RE-TM alloys<sup>22,23</sup>. The demagnetization field  $\vec{H}_{DM}$  points opposite the local magnetization when magnetization is oriented out-of-plane in a thin film geometry. This is insufficient to reverse the magnetization at room temperature. However, when the coercive field is reduced in the regions heated by the laser spot,  $\vec{H}_{DM}$  can reverse the magnetization [Fig. 7(b)]. This may be compared to thermomagnetic writing done with an external field  $\vec{H}_{ext}$ , which is no longer required.

When  $\sigma_w$  and  $M_s^2$  in Eq. (2) have different temperature dependencies, domains will expand or contract, depending on the temperature, which can explain the growth of domains away from the area directly under the laser beam. For instance, if  $\sigma_w$  decreases faster with  $T$  than  $M_s^2$ , the wall energy is relatively smaller and the domain expands. Then, a time-dependent temperature  $T(t)$  will give a time-dependent domain size, moving DW from the area directly under the laser beam. In addition, temperature gradients  $\frac{\partial T(x,t)}{\partial x}$  near the laser beam can also give a force on domain walls. A temperature

gradient introduces spatial gradients in  $\sigma_w$  and  $M_s$  and therefore in the energy of Eq. (2)<sup>28</sup>. This gives a force that can either pull the domain toward the laser spot, or push it away.

When DW are easier to move at large temperature than at lower temperature, the DW motion is not reversible and domains do not contract back on cooling once the laser beam moves away. Domain nucleation and DW motion can be repeated once the first wall has moved away from the nucleation area and  $H_{DM}$  is again sufficiently high to nucleate a new domain of opposite magnetization, as seen in the additional reversal at stripe center [Fig. 2(c)].

Propagation of domain walls away from the writing area, heat accumulation and diffusion, make the quantitative analysis of the results when the beam is moved on the sample a complicated and challenging problem. A time-dependent  $T(x, t)$ , determined by heat diffusion, writing and beam parameters, together with time-dependent T gradients in the film along and normal to the scan direction, can qualitatively explain the dependence of the DW orientation on scanning direction (Fig. 5).

The presented images were made long after the cumulative AOS process was complete and many questions remain. Multiple processes at different timescales take part: single-pulse laser heating (a few  $ps$ ), heat accumu-

lation ( $ms$  range), single-pulse substrate cooling ( $\mu s$ ), domain wall processes ( $\mu s$ ). Slower (not precession or DW based) dynamics may also play a role ( $ms - s$ ). What is the high-resolution quantitative dynamics of the AOS process? Time-resolved imaging with a triggered CCD camera and, in another time range, with a delayed ultrafast probe pulse will address these questions.

#### IV. CONCLUSION

Cumulative all-optical switching in ferromagnetic Co/Pd superlattices supports a thermally-induced reversal and the importance of long-range magnetic interactions. Lattice participates in the reversal for our experimental conditions. Once switching is initiated, a relatively slow domain evolution follows. Intriguing questions remain on the high-resolution dynamics of the observed magnetization switching.

#### V. ACKNOWLEDGMENTS

This research was supported by the University of Louisville Research Foundation.

---

<sup>1</sup> C. D. Stanciu, F. Hansteen, A.V. Kimel, A. Kirilyuk, A. Tsukamoto, A. Itoh, and Th. Rasing, Phys. Rev. Lett. **99**, 047601 (2007)

<sup>2</sup> A. Ashkin and J.M. Dziedzic, Appl. Phys. Lett. **21**(6), 253 (1972)

<sup>3</sup> M. Kaneko, T. Okamoto, H. Tamada, and T. Yamada, IEEE Transactions on Magnetics **22**(1), 2 (1986)

<sup>4</sup> K. Vahaplar, A. M. Kalashnikova, A. V. Kimel, S. Gerlach, D. Hinzke, U. Nowak, R. Chantrell, A. Tsukamoto, A. Itoh, A. Kirilyuk, and Th. Rasing, Phys. Rev. B **85**, 104402 (2012)

<sup>5</sup> A. R. Khorsand, M. Savoini, A. Kirilyuk, A.V. Kimel, A. Tsukamoto, A. Itoh, and Th. Rasing, Phys. Rev. Lett. **108**, 127205 (2012)

<sup>6</sup> I. Tudosa, C. Stamm, A. B. Kashuba, F. King, H. C. Siegmann, J. Stohr, G. Ju, B. Lu, and D. Weller, Nature 428, 831 (2004)

<sup>7</sup> U. Atxitia, P. Nieves, and O. Chubykalo-Fesenko, Phys. Rev. B **86**, 104414 (2012)

<sup>8</sup> T.A. Ostler, J. Barker, R.F.L. Evans, R.W. Chantrell, U. Atxitia, O. Chubykalo-Fesenko, S.El Moussaoui, L. Le Guyader, E. Mengotti, L.J. Heyderman, F. Nolting, A. Tsukamoto, A. Itoh, D. Afanasiev, B.A. Ivanov, A.M. Kalashnikova, K. Vahaplar, J. Mentink, A. Kirilyuk, Th. Rasing and A.V. Kimel, Nat. Comm. (2012)

<sup>9</sup> E. Oniciuc, L. Stoleriu, D. Cimpoesu, and A. Stancu, Appl. Phys. Lett. **104**, 222404 (2014)

<sup>10</sup> C-H. Lambert, S. Mangin, B. S. D. Ch. S. Varaprasad, Y. K. Takahashi, M. Hehn, M. Cinchetti, G. Malinowski, K. Hono, Y. Fainman, M. Aeschlimann, and E. E. Fullerton, Science **345**, 1337 (2014)

<sup>11</sup> M.S. El Hadri, P. Pirro, C.-H. Lambert, S. Petit-Watelot, Y. Quessab, M. Hehn, F. Montaigne, G. Malinowski, and S. Mangin, arXiv:1602.08525v2 (2016)

<sup>12</sup> M. Stark, F. Schlickeiser, D. Nissen, B. Hebler, P. Graus, D. Hinzke, E. Scheer, P. Leiderer, M. Fonin, M. Albrecht, U. Nowak, and J. Boneberg, Nanotechnology **26**, 205302 (2015)

<sup>13</sup> V. R. Bhardwaj, E. Simova, P. P. Rajeev, C. Hnatovsky, R. S. Taylor, D. M. Rayner, and P. B. Corkum, Phys. Rev. Lett. **96**, 057404 (2006)

<sup>14</sup> G. Cheng, K. Mishchik, C. Mauclair, E. Audouard, and R. Stoian, Optics Express **17**, 9515 (2009)

<sup>15</sup> L. Sudrie, M. Franco, B. Prade, and A. Mysyrowicz, Opt. Comm. **191**, 333 (2001)

<sup>16</sup> P. Yang, G. R. Burns, J. Guo, T. S. Luk, and G. A. Vawter, J. Appl. Phys. **95**, 5280 (2004)

<sup>17</sup> B. Koopmans, J. J. M. Ruigrok, F. Dalla Longa, and W. J. M. de Jonge, Phys. Rev. Lett. **95**, 267207 (2005)

<sup>18</sup> S. Gunther, C. Spezzani, R. Cipriani, C. Grazioli, B. Ressel, M. Coreno, L. Poletto, P. Miotti, M. Sacchi, G. Panaccione, V. Uhli, E. E. Fullerton, G. De Ninno, and Ch. H. Back, Phys. Rev. B **90**, 180407(R) (2014)

<sup>19</sup> K. C. Kuiper, T. Roth, A. J. Schellekens, O. Schmitt, B. Koopmans, M. Cinchetti, and M. Aeschlimann, Appl. Phys. Lett. **105**, 202402 (2014)

<sup>20</sup> A. J. Schmidt, X. Chen, and G. Chen, Rev. Sci. Instr. **79**, 114902 (2008)

<sup>21</sup> B. Koopmans, M. van Kampen, J. T. Kohlhepp, and W. J. M. de Jonge, Phys. Rev. Lett. **85**, 844 (2000)

<sup>22</sup> H-P. D. Shieh and M. H. Kryder, *Appl. Phys. Lett.* **49**(8), 473 (1986)

<sup>23</sup> H-P. D. Shieh and M. H. Kryder, *J. Appl. Phys.* **61**(3), 1108 (1987)

<sup>24</sup> C. H. Back, R. Allenspach, W. Weber, S. S. P. Parkin, D. Weller, E. L. Garwin, and H. C. Siegmann, *Science* **285**, 864 (1999)

<sup>25</sup> M. Bauer, R. Lopusnik, J. Fassbender, and B. Hillebrands, *J. of Magn. and Magn. Mat.* **218**, 165 (2000)

<sup>26</sup> H.W. Schumacher, C. Chappert, R. C. Sousa, P. P. Freitas, and J. Miltat, *Phys. Rev. Lett.* **90**, 017204 (2003)

<sup>27</sup> Th. Gerrits, H. A. M. van den Berg, J. Hohlfeld, L. Bar, and Th. Rasing, *Nature* **418**, 509 (2002)

<sup>28</sup> A. A. Thiele, A. H. Bobeck, E. Della Torre, and U. F. Gianola, *Bell Syst. Tech. Journal* **50**(3), 711 (1971)